



# Photophysicochemical behaviour of anionic indium phthalocyanine when grafted onto $\text{Ag}_x\text{Au}_y$ and porous silica nanoparticles



Edith Dube, David O. Oluwole, Tebello Nyokong\*

Department of Chemistry, Rhodes University, Grahamstown 6140, South Africa

## ARTICLE INFO

### Keywords:

Silica nanoparticles  
Indium phthalocyanine  
Triplet quantum yields  
Gold-silver nanoalloy

## ABSTRACT

This work reports on the synthesis of glutathione functionalised  $\text{Ag}_3\text{Au}_1$  (Ag rich alloy, denoted as AgAu) and  $\text{Ag}_1\text{Au}_3$  (Au rich alloy – denoted as AuAg) nano alloys as well as aminopropyl triethoxysilane capped  $\text{Ag}_1\text{Au}_3$  doped silica nanoparticles (NPs). The NPs were covalently linked to indium(III) chloride 2,9(10),16(17),23(24)-tetra-(3-carboxyphenoxy)phthalocyanine (**1**) via amide bond to form **1**-AgAuNPs-GSH and **1**-AuAgNPs-GSH. The AgAuNPs were also doped into aminopropyl triethoxysilane (APTES) silica NPs (SiNPs-APTES) followed by linkage to complex **1** to form **1**-AgAu-SiNPs-APTES. The photophysicochemical behaviour of complex **1** and its nanoconjugates were investigated. Decrease in the fluorescence quantum yield and lifetimes was observed in the conjugates in comparison to **1** alone. The singlet oxygen quantum yield for **1**-AgAuNPs-GSH and **1**-AuAgNPs-GSH decreased probably due to the screening effect caused by the NPs, while that of **1**-AgAu-SiNPs-APTES increased in dimethylsulfoxide probably due to the permeability of the porous silica matrix to molecular oxygen.

## 1. Introduction

Metallophthalocyanines (MPcs) are well known as photosensitizers for photodynamic therapy (PDT) [1–3] due to their ability to efficiently generate singlet oxygen. Photodynamic therapy (PDT) is a cancer treatment which requires a photosensitizer and light of appropriate wavelength in the presence of ground state molecular oxygen to elicit selective destruction of the tumor cells [1].

On the other hand, the fabrication of gold-silver alloy nanoparticles is receiving considerable attention due to the tunability of their surface plasmon resonance (SPR) band [4,5] resulting in applications in many areas such as in non-linear optics [6–8], biomedicine [9], catalysis [10,11] and bio-imaging [12,13]. Gold nanoparticles (AuNPs) have been separately (not as an alloy) linked to MPcs for PDT applications [14–16] and for improved singlet oxygen generation [17,18]. Silver nanoparticles (AgNPs) have also been linked to MPcs with improved triplet state and singlet oxygen quantum yields [19]. Improved triplet state quantum yields were observed for a non-water soluble ZnPc derivative when linked (via N- or S-metal bond) to AuAg alloyed nanoparticles [20]. The improved triplet state behaviour of MPcs in the presence of Au/Ag NPs is due to the heavy atom effect of the latter which enhances intersystem crossing to the triplet state of the Pc.

In the current work glutathione functionalised  $\text{Ag}_3\text{Au}_1$  and  $\text{Ag}_1\text{Au}_3$  nano-alloys as well as aminopropyl triethoxysilane (APTES) capped

$\text{Ag}_3\text{Au}_1$  doped into silica nanoparticles (SiNPs) were synthesized. The numbers refer to the ratios of Au and Ag. The Ag rich alloy ( $\text{Ag}_3\text{Au}_1$ ) is denoted as AgAu, and the Au rich alloy ( $\text{Ag}_1\text{Au}_3$ ) is denoted as AuAg throughout the manuscript. The NPs are denoted as AgAuNPs-GSH, AuAgNPs-GSH, and AgAu-SiNPs-APTES. The NPs were covalently linked to indium(III) chloride 2,9(10),16(17),23(24)-tetra-(3-carboxyphenoxy)phthalocyanine (**1**) via amide bond formation for the first time. The conjugates are denoted as **1**-AgAuNPs-GSH, **1**-AuAgNPs-GSH, and **1**-AgAu-SiNPs-APTES, respectively. The resulting conjugates are water soluble and hence are appropriate for applications in biological media. Indium was used as a central metal due to its heavy atom effect which leads to improved triplet state parameters.

In this work AgAuNPs are doped onto SiNPs for the first time and linked to a Pc resulting in improved singlet oxygen quantum yield (in DMSO), which is important for PDT applications. The porous silica structure acts as a suitable carrier for hydrophobic molecules and can also protect the loaded molecules from degradation [21].

The MPc, NPs and the conjugates were characterized and the photophysicochemical properties were evaluated.

\* Corresponding author.

E-mail address: [t.nyokong@ru.ac.za](mailto:t.nyokong@ru.ac.za) (T. Nyokong).

## 2. Experimental

### 2.1. Materials

Ultra-pure water was obtained from a Milli-Q Water System (Millipore Corp, Bedford, MA, USA), KOH, gold(III) chloride hydrate, glutathione (GSH), silver acetate, oleic acid (OA), oleylamine (OLA), N,N'-dicyclohexylcarbodiimide (DCC), 4-(dimethylamino)pyridine (DMAP), zinc phthalocyanine (ZnPc), Triton X-100, tetraethyl orthosilicate (TEOS), 1,3-diphenylisobenzofuran (DPBF), anthracene-9,10-bis-methylmalonate (ADMA), and aminopropyl triethoxysilane (APTES) were purchased from Sigma-Aldrich. NH<sub>3</sub>OH (25%), tetrahydrofuran (THF), N,N-dimethyl formamide (DMF) and dimethyl sulphoxide (DMSO) were purchased from Merck. Absolute ethanol (EtOH) was obtained from SAARCHEM. All other reagents and solvents were obtained from commercial suppliers and used as received. AlPcSmix (containing a mixture of sulfonated derivatives), and used as a standard for singlet oxygen quantum yields in water, was synthesized as reported in literature [22]. Indium(III) chloride 2,9(10),16(17),23(24)-tetra-(3-carboxyphenoxy) phthalocyanine (**1**) was synthesized and purified as reported in the literature [23].

### 2.2. Equipment

Infrared spectra were acquired on a Bruker ALPHA FT-IR spectrometer with universal attenuated total reflectance (ATR) sampling accessory. X-ray powder diffraction patterns were recorded using a Cu K radiation (1.5405 Å, nickel filter), on a Bruker D8 Discover equipped with a proportional counter and the data was processed using the Eva (evaluation curve fitting) software. The morphologies of the nanoalloys and their conjugates were assessed using a transmission electron microscope (TEM), ZEISS LIBRA model 120 operated at 90 kV and iTEM software was used for TEM micrographs processing. Elemental compositions of the NPs and the nanoconjugates were qualitatively determined using energy dispersive X-ray spectroscopy (EDX), INCA PENTA FET coupled to the VAGA TESCAME operated at 20 kV accelerating voltage. Ground state electronic absorption spectra were measured using a Shimadzu UV-2550 spectrophotometer. Fluorescence excitation and emission spectra were measured on a Varian Eclipse spectrofluorimeter using a 360–1100 nm filter. Excitation spectra were recorded using the Q-band of the emission spectra. Fluorescence lifetimes were measured using a time correlated single photon counting setup (TCSPC) (FluoTime 300, Picoquant GmbH) with a diode laser (LDH-P-670, Picoquant GmbH, 20 MHz repetition rate, 44 ps pulse width). Details have been provided before [24].

Triplet quantum yields were determined using a laser flash photolysis system. The excitation pulses were produced using a tunable laser system consisting of an Nd:YAG laser (355 nm, 135 mJ/4–6 ns) pumping an optical parametric oscillator (OPO, 30 mJ/3–5 ns) with a wavelength range of 420–2300 nm (NT-342B, Ekspla), as reported before [24].

Irradiation for singlet oxygen quantum yield was performed using a general electric quartz lamp (300 W) as described in the literature [23]. Light intensity was measured with a POWER MAX 5100 (Molelectron® detector incorporated) power meter and was found to be  $4.3 \times 10^{15}$  photons cm<sup>-2</sup> s<sup>-1</sup>.

X-ray photoelectron spectroscopy (XPS) analysis was done using an AXIS Ultra DLD, with Al (monochromatic) anode equipped with a charge neutraliser, supplied by Kratos Analytical. The following parameters were used: the emission was 10 mA, the anode (HT) was 15 kV and the operating pressure below  $5 \times 10^{-9}$  torr. A hybrid lens was used and resolution to acquire scans was at 160 eV pass energy in slot mode. The centre used for the scans was at 520 eV with a width of 1205 eV, steps at 1 eV and dwell time at 100 ms as. The high resolution scans were acquired using 80 eV pass energy in slot mode.

### 2.3. Syntheses

#### 2.3.1. AgAu alloy nanoparticles (oleic acid, OA, and oleylamine, OLA capped), Scheme 1A

AgAu nano-alloys with different mole ratios (3:1 and 1:3) were synthesized as reported in literature with modifications [20]. For the formation of Ag<sub>3</sub>Au<sub>1</sub> (this is a Ag rich alloy denoted as AgAu in this work), a mixture of silver acetate (0.38 g, 2.26 mmol) and HAuCl<sub>4</sub>·3H<sub>2</sub>O (0.251 g, 0.74 mmol) was employed. For the formation of Ag<sub>1</sub>Au<sub>3</sub> (this is an Au rich alloy denoted as AuAg in this work), a mixture of silver acetate (0.062 g, 0.37 mmol) and HAuCl<sub>4</sub>·3H<sub>2</sub>O (0.38 g, 1.11 mmol) was employed. The mixtures above were separately placed into 250 mL round bottom flasks containing diphenyl ether (30 g, 176.3 mmol), oleylamine (OLA, 10 mL) and oleic acid (OA, 5 mL). The reaction mixtures were refluxed at 160 °C and maintained under argon atmosphere for 5 h, followed by cooling to ambient temperature. The products were successively purified with ethanol and dried in enclosed fume hood and are represented as AgAuNPs-OA/OLA and AuAgNPs-OA/OLA.

#### 2.3.2. Glutathione (GSH) functionalization of AgAuNPs and AuAgNPs-Scheme 1A

The surface of the AgAuNPs and AuAgNPs were separately modified with glutathione (GSH) as follows: AgAuNPs-OA/OLA or AuAgNPs-OA/OLA (0.40 g) were each transferred into two separate round bottom flasks containing chloroform (3 mL). A solution containing methanol (20 mL), GSH (0.25 g, 0.81 mmol) and KOH (0.50 g, 8.93 mmol) was added to the NPs mixture. The mixtures were allowed to stir for 2 h at ambient temperature. Afterwards, the formed GSH capped NPs were precipitated out of solution using ethanol, and purified with methanol. The obtained solid precipitates were air dried in an enclosed fume hood. The nanoparticles are represented as AgAuNPs-GSH and AuAgNPs-GSH.

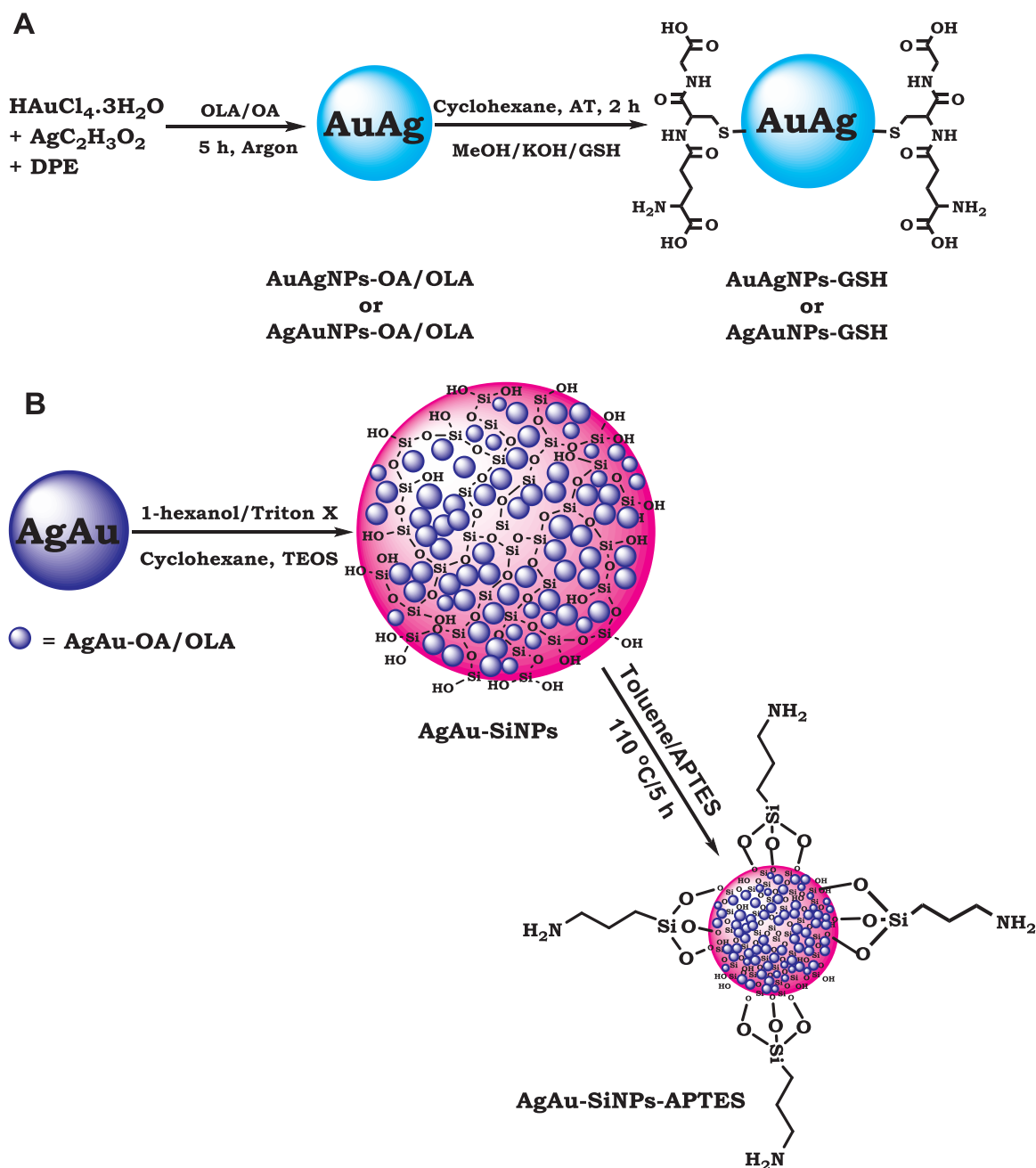
#### 2.3.3. Doping of AgAuNPs-OA/OLA into SiNPs to form AgAu-SiNPs-APTES, Scheme 1B

The doping of the AgAuNPs into SiNPs was done using a method adopted from literature [25] as follows: Triton X-100 (1.80 mL), 1-hexanol (1.80 mL) and cyclohexane (7.5 mL) were introduced into a 50 mL round bottom flask and stirred for 20 min. Afterwards 0.20 g of AgAuNPs-OA/OLA in cyclohexane was added and the mixture was further stirred for 10 min. TEOS (0.15 mL) was then added, followed by dropwise addition of H<sub>2</sub>O (0.4 mL) and 25% NH<sub>3</sub>OH solution (0.06 mL) for 1 h. The mixture was kept stirring for 24 h to allow for nucleation and particle growth of the SiNPs around AgAuNPs to form AgAu-SiNPs. The obtained product was isolated out of solution using ethanol, purified with ethanol and air dried in an enclosed fume hood.

The functionalisation of the AgAu-SiNPs using APTES was done as reported in the literature [26] with modifications. Briefly, 0.09 g of AgAu-SiNPs was weighed into a 50 mL round bottom flask, then, APTES (0.2 mL, 0.85 mmol) and toluene (2 mL) were added. The mixture was refluxed at 110 °C for 5 h. The obtained product was purified with ethanol and acetonitrile. Finally, the solid was air dried in an enclosed fume hood and stored for further characterization. The product is represented as AgAu-SiNPs-APTES.

#### 2.3.4. Conjugation of complex 1 to NPs (Scheme 2)

The phthalocyanine-NPs conjugates were synthesized as follows: complex **1** (0.02g, 0.017 mmol) was dissolved in 2 mL of dry DMF. Then DCC (0.01 g, 0.049 mmol) and DMAP (0.005 g, 0.042 mmol) were added and the resulting solution was stirred for 48 h. The coupling agents were added to activate the carboxylic acid group of **1**, to allow for covalent linkage of **1** to NPs via amide bond formation. Afterwards, 0.05 g of AuAgNPs-GSH was added and the reaction mixture was stirred for a further 48 h at ambient temperature. The same protocol was employed for AgAuNPs-GSH and AgAu-SiNPs-APTES. The



**Scheme 1.** Synthetic pathways for (A) AuAgNPs-GSH and (B) AgAu-SiNPs-APTES.

conjugates (1-AuAgNPs-GSH, 1-AgAuNPs-GSH and 1-AgAu-SiNPs-APTES) were centrifuged, successively purified with ethanol and allowed to dry in the fume hood.

#### 2.4. Photophysicochemical studies

Fluorescence ( $\Phi_F$ ) and triplet ( $\Phi_T$ ) quantum yields of the complex **1** alone or in conjugation with NPs were determined in DMSO and in aqueous media (for  $\Phi_F$  only) using comparative methods described before in the literatures [27–29]. Unsubstituted ZnPc in DMSO was used as a standard with  $\Phi_F = 0.20$  [28] and  $\Phi_T = 0.65$  [29]. The solutions for triplet state studies were de-aerated with argon for 15 min before measurements.

Singlet oxygen quantum yield ( $\Phi_{\Delta}$ ) values were determined under ambient conditions using DPBF as a singlet oxygen quencher in DMSO (and ADMA in water) and equations described before [30,31]. ZnPc was

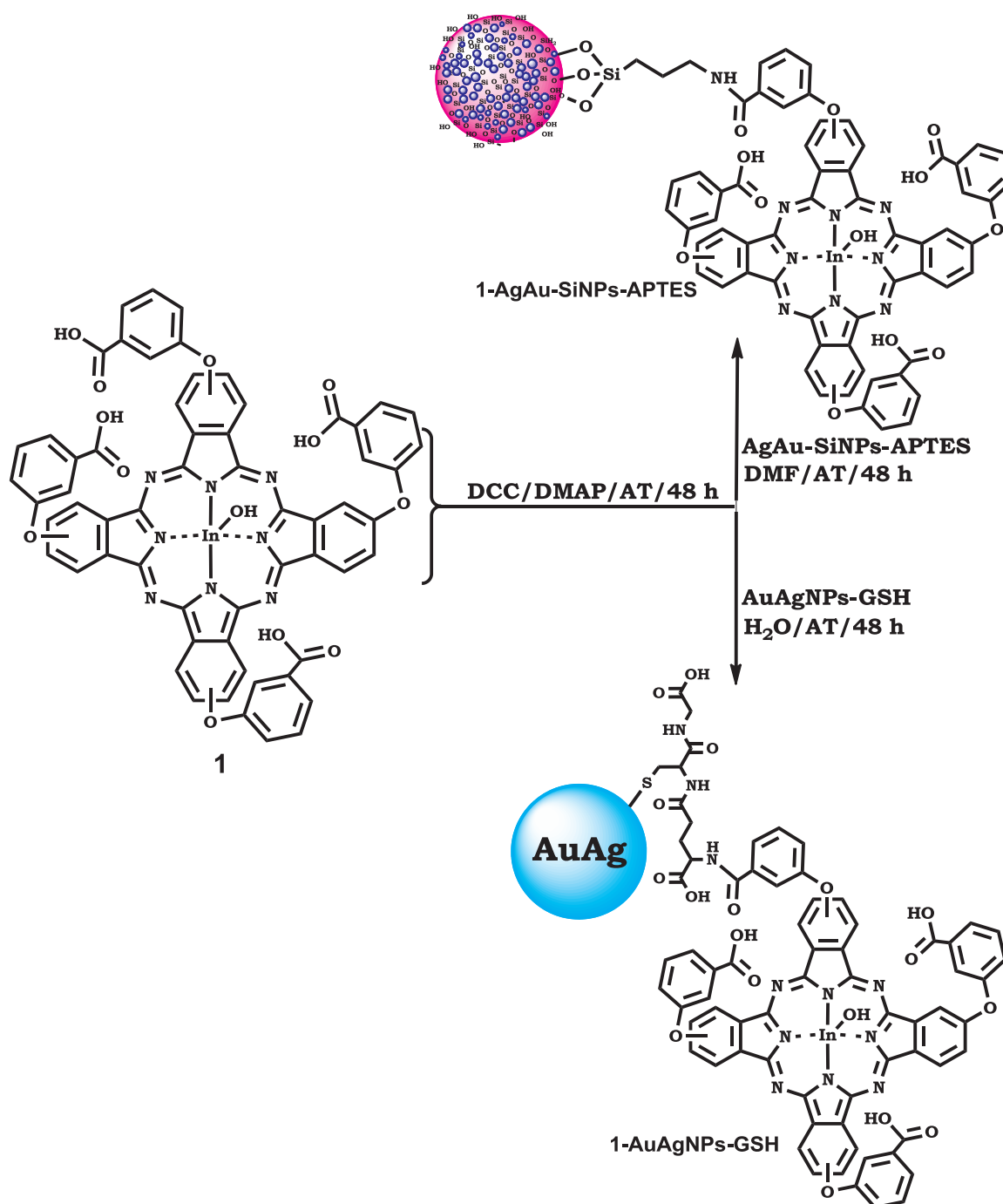
used as a standard ( $\Phi_{\Delta(\text{Std})} = 0.67$  in DMSO [30]). AlPcSmix was employed as a standard in aqueous media ( $\Phi_{\Delta(\text{Std})} = 0.42$  [32]). The absorbances of DPBF or ADMA were spectroscopically monitored at 417 nm or 380 nm respectively at a predetermined time course.

### 3. Results and discussion

#### 3.1. Characterization of NPs and conjugates

**Scheme 1** shows the synthetic pathway for AuAgNPs-GSH and AgAuNPs-GSH (**A**) and AgAu-SiNPs-APTES (**B**). **Scheme 2** shows the covalent linkage of complex **1** to AgAu-SiNPs-APTES and AuAgNPs-GSH (as representatives).

Complex **1** and 1-AgAu-SiNPs-APTES are not readily soluble in water and are slightly soluble in 1 M NaOH, thus for studies in water these were first dissolved in a few drops of DMSO and then diluted with



**Scheme 2.** Synthetic pathway for covalent linkage of complex 1 to AgAu-SiNPs-APTES and AuAgNPs-GSH to form 1-AgAu-SiNPs-APTES and 1-AuAgNPs-GSH (AuAgNPs-GSH represents AgAuNPs-GSH also).

water. 1-AuAgNPs-GSH and 1-AgAuNPs-GSH are readily soluble in water which is important for practical applications.

### 3.1.1. UV/vis absorption and emission spectra

The surface plasmon peaks of AgAuNPs-GSH (Fig. 1b) and AuAgNPs-GSH (Fig. 1a) were observed at 410 nm and 506 nm in DMSO, respectively. The SPR peaks of the alloys are very close to the SPR positions of individual AgNPs and AuNPs, depending on the composition of Ag or Au present in the alloys [5].

No significant absorption peak was observed for AgAuNPs in the AgAuNPs-SiNPs-APTES which could be attributed to successful doping of the NPs into SiNPs (Fig. 1c). Hence the AgAuNPs are not exposed and do not show the SPR band. This confirms that the AgAuNPs are

embedded within the SiNPs.

In DMSO complex 1 is not aggregated as judged by a single narrow Q band in the UV/Vis spectra, Fig. 2A. In aqueous media complex 1 and its conjugates with AgAuNPs or AuAgNPs (Fig. 2B) shows very weak broad Q bands. This is typical of Pcs in aqueous solution and is attributed to aggregation [33]. For Pcs, aggregation is due to  $\pi$ - $\pi$  stacking interaction of the aromatic rings. Aggregation is highly reduced in 1-AgAu-SiNPs-APTES in water, Fig. 2B, with a relatively narrower and intense Q band, most likely due to the presence of small amounts of DMSO. Organic solvents break aggregates in Pc complexes. The B band is also intense and well defined in 1-AgAu-SiNPs-APTES, Fig. 2B.

Slight blue shifts in the Q band of 1 in the nanoconjugates (except for 1-AgAu-SiNPs-APTES in DMSO) were observed in both DMSO and

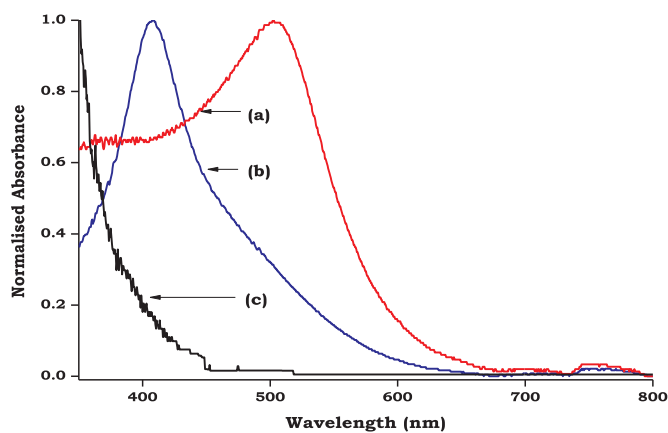


Fig. 1. Normalized absorption spectra for AuAgNPs-GSH (a), AgAuNPs-GSH (b), and AgAu-SiNPs-APTES (c). AgAuNPs-GSH (a), and AuAgNPs-GSH (b) were measured in water and AgAu-SiNPs-APTES (c) was measured in DMSO.

water (Fig. 2A, Table 1). The slight blue shifts upon conjugation of the NPs to **1** could be attributed to the electron deficiency induced on the Pcs upon coordination with NPs as reported before [34]. Phthalocyanines do not display any significant absorbance between the Soret band and the Q band; however on conjugation to AgAuNPs or AuAgNPs, there was increased absorption between the Soret and the Q band corresponding to the SPR band for both the AuAgNPs-GSH and AgAuNPs-GSH confirming their conjugation to **1**, in DMSO and water. The 1-AgAu-SiNPs-APTES spectra (Fig. 2A and B) do not show these SPR bands as also observed for AgAu-SiNPs-APTES alone. Since complex **1** is linked to the surface of the SiNPs in 1-AgAu-SiNPs-APTES, its spectrum is observed while the SPR bands are not observed.

Fig. 2C shows the absorption, emission and excitation spectra of 1-AgAu-SiNPs-APTES as an example. The emission spectrum is weak due to the combined heavy atom effect of the central ion and the nanoparticles. The ground state electronic absorption and excitation spectra of Pcs are usually similar; however the Pc nano-conjugates displayed slight differences which could be attributed to change in molecular geometry upon excitation [35].

### 3.1.2. FT-IR spectra

FT-IR spectra were used for the assessment of functional groups present on **1**, NPs and their nanoconjugates. The FT-IR spectrum of GSH (Fig. 3A(c)) showed a peak at  $2515\text{ cm}^{-1}$  (SH) but on functionalization of the NPs, the disappearance of the thiol peak was observed due to linkage of the GSH to the metal surface of the NPs (Fig. 3A(b), using AuAg as an example). The appearance of a very broad peak at  $3171\text{ cm}^{-1}$  (OH/NH) in Fig. 3A(b) (AuAgNPs-GSH) show the presence of the carboxylic hydroxyl and amine (NH) groups, while split peaks at  $1632\text{ cm}^{-1}$  and  $1532$  are characteristic of primary amines. The

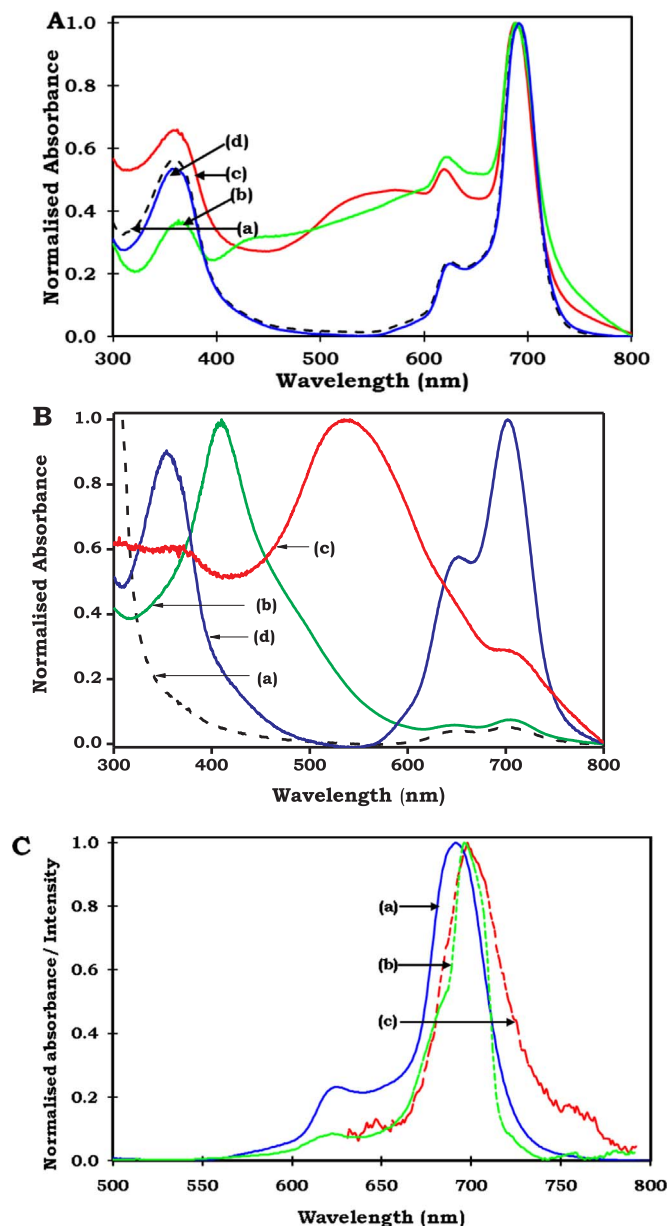


Fig. 2. Normalized overlay absorption spectra (A) in DMSO and (B) in water of complex **1** (a), 1-AgAuNPs-GSH (b), 1-AuAgNPs-GSH (c), and 1-AgAuNPs-SiNPs-APTES (d). (C) Absorption (a), excitation (b) and emission (c) spectra of 1-AgAu-SiNPs-APTES (excitation = 612 nm, solvent = DMSO).

Table 1

Photophysical parameters of nanoconjugates of complex **1** in DMSO (Excitation at 612 nm).

Samples <sup>a</sup>	$\lambda_{\text{abs}}^b$ (nm)	$\Phi_F^b$	$\tau_F$ (ns) (%)	Mean $\tau_F$ (ns)	$\Phi_T$	$\tau_T$ ( $\mu\text{s}$ )	$\Phi_{\Delta}^b$ ( $\pm 0.01$ )
<b>1</b>	691 (708)	0.015 (< 0.01)	2.43 (100)	2.43	0.65	58	0.37 (0.16)
1-AuAgNPs-GSH (18.9 nm) <sup>a</sup>	687 (704)	< 0.01 (< 0.01)	0.32 (51) 3.26 (49)	1.75	0.79	73	0.27 (0.11)
1-AgAuNPs-GSH (15.1 nm) <sup>a</sup>	689 (705)	< 0.01 (< 0.01)	0.34 (78) 3.27 (22)	0.98	0.73	58	0.25
1-AgAu SiNPs-APTES (11.4 nm) <sup>a</sup>	691 (702)	0.010 (< 0.01)	0.31 (81) 5.15 (19)	1.25	0.55	81	0.49 (0.15)

<sup>a</sup> Numbers in brackets are the sizes (from XRD) of the NPs before conjugation to complex **1**.

<sup>b</sup> Values in water in brackets.

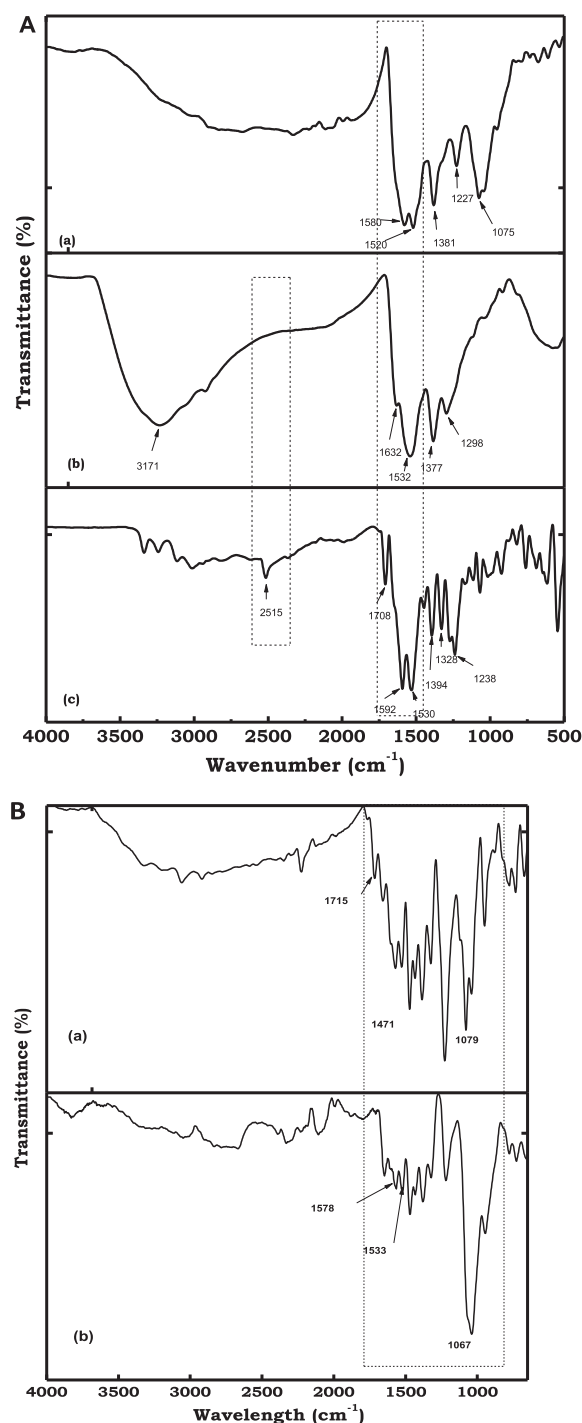


Fig. 3. FT-IR spectra of (A) 1-AuAgNPs-GSH (a), AuAgNPs-GSH (b), and GSH alone (c); and (B) complex 1 (a), and 1-AgAu-SiNPs-APTES (b).

appearance of the secondary carbonamide ( $\text{O}=\text{C}-\text{NH}$ ) band at  $1580\text{ cm}^{-1}$  (Fig. 3A(a)), with the disappearance of the primary amine peaks suggests the linkage of the glutathione functionalised nanoparticles to **1** through the amide bond. The same trend was observed for the 1-AgAuNPs-GSH.

The FT-IR spectrum of the 1-AgAu-SiNPs-APTES (Fig. 3B(b)) shows the presence of peaks at  $1533$  and  $1578\text{ cm}^{-1}$ , due to the amide bond formation ( $\text{O}=\text{C}-\text{NH}$ ). This suggests successful formation of a bond between AgAu-SiNPs-APTES and **1**. In addition, the spectrum showed the presence of the siloxane band at  $1067\text{ cm}^{-1}$  which is typical of SiNPs.

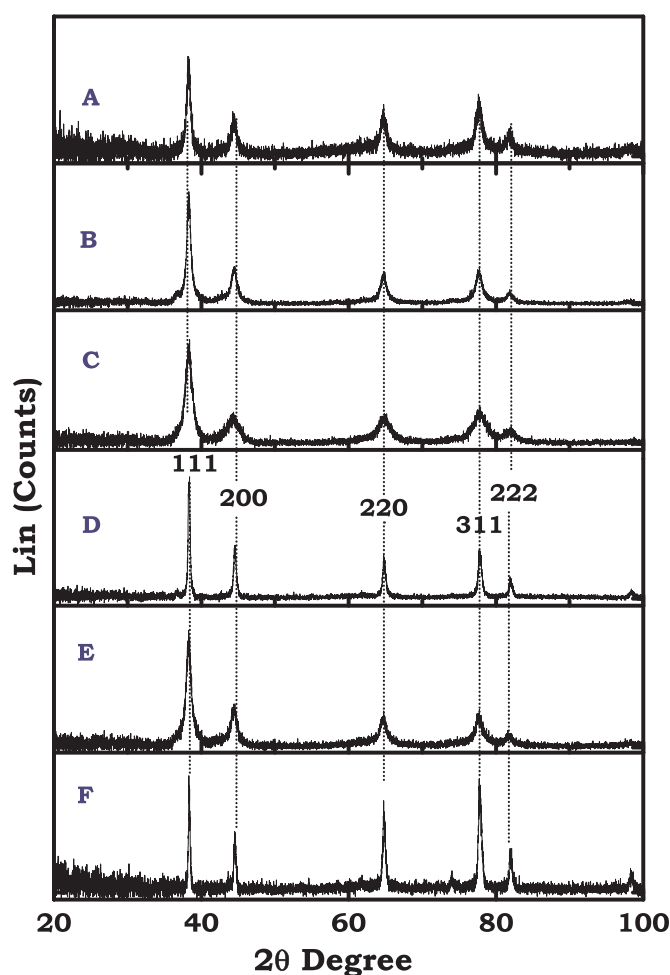


Fig. 4. XRD diffractograms for 1-AgAu-SiNPs-APTES (A), AgAu-SiNPs-APTES (B), 1-AuAgNPs-GSH (C), AuAgNPs-GSH (D), 1-AgAuNPs-GSH (E), and AgAuNPs-GSH (F).

### 3.1.3. XRD studies

Fig. 4 shows the X-ray diffraction (XRD) patterns of the silver and gold nano-alloys, and their conjugates. Both the NPs and their conjugates displayed a powder diffraction pattern resembling a face centered cubic crystal (FCC) structure, characteristic of gold and silver [36,37]. The XRD displayed peaks at  $2\theta = 38.4^\circ, 44.7^\circ, 64.9^\circ, 77.6^\circ$  and  $81^\circ$ .

Scherrer Eq. (1) [38] was employed for the estimation of the sizes of the NPs:

$$d = \frac{k\lambda}{\beta \cos \theta} \quad (1)$$

where  $\lambda$  is the wavelength of the X-ray source ( $1.5405\text{ \AA}$ ),  $k$  is an empirical constant equal to 0.9,  $\beta$  is the full width at half maximum of the diffraction peak and  $\theta$  is the angular position. The sizes were estimated to  $15.1\text{ nm}$  for AgAuNPs-GSH,  $18.9\text{ nm}$  for AuAgNPs-GSH and  $11.4\text{ nm}$  for AgAu-SiNPs-APTES (Fig. 4). It is important to note that XRD pattern is observed for AgAu within AgAu-SiNPs-APTES while the SPR band was not observed. This is due to the penetrating nature of the XRD. The XRD data does confirm the presence of AgAu within the SiNPs.

### 3.1.4. TEM

Fig. 5 shows the TEM micrographs for AuAgNPs-GSH, 1-AuAgNPs-GSH, AgAuNPs-GSH, 1-AgAuNPs-GSH, AgAu-SiNPs-APTES, and 1-AgAu-SiNPs-APTES. The NPs were relatively monodispersed but high aggregation was observed on the nanoconjugates, possibly due to  $\pi$ - $\pi$  stacking between the Pcs on adjacent nanoparticles. Pcs are known for their  $\pi$ - $\pi$  stacking to form H aggregates [33]. The average size of the

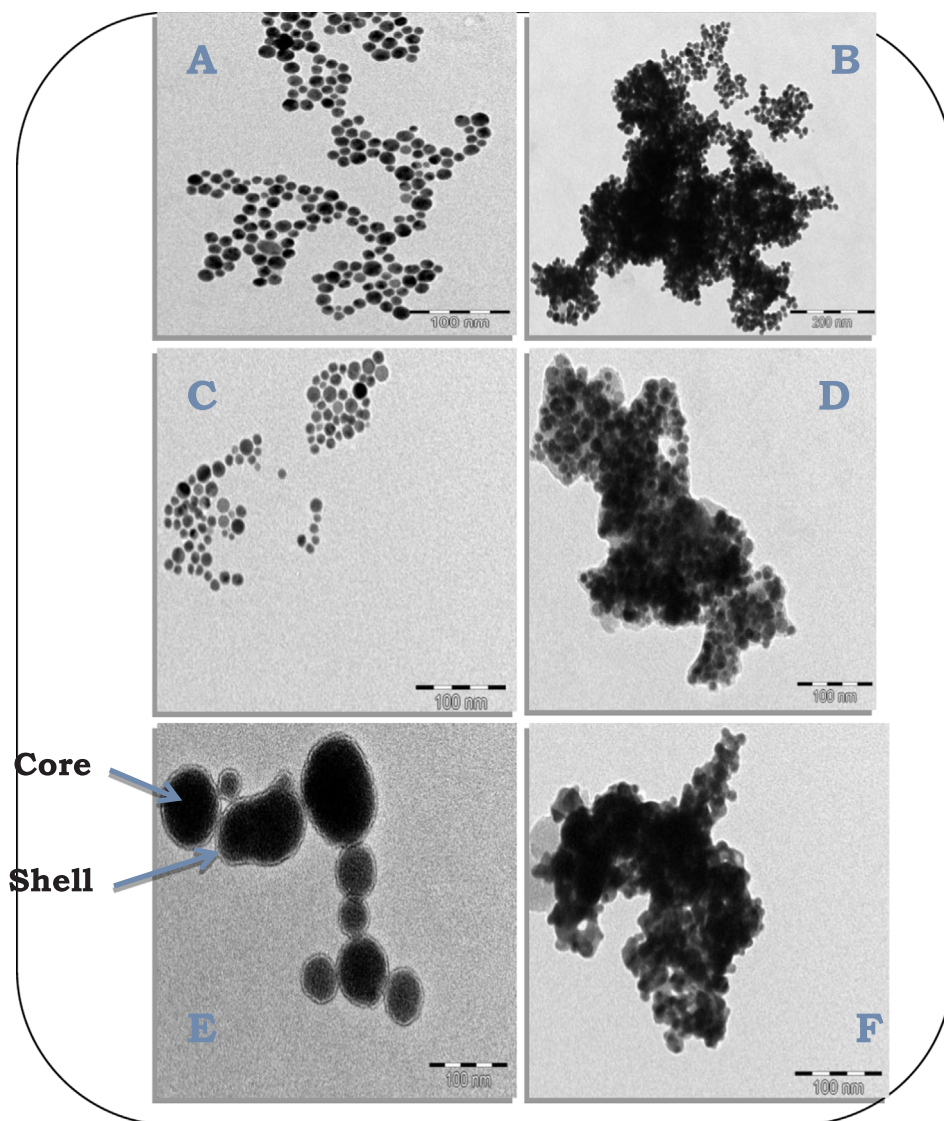


Fig. 5. TEM micrographs for AgAuNPs-GSH (A), 1-AgAuNPs-GSH (B), AuAgNPs-GSH (C), 1-AuAgNPs-GSH (D), AgAu-SiNPs-APTES (E), and 1-AgAu-SiNPs-APTES (F).

NPs was estimated to be 11.7 nm and 10.5 nm for AgAuNPs-GSH and AuAgNPs-GSH, respectively. The sizes are smaller than obtained by XRD above. The TEM image of the AgAu-SiNPs-APTES, Fig. 5E, shows a central dark region with a light ring around it, an indication that silica has formed a coat on the AgAuNPs surface.

### 3.1.5. EDX spectra

Qualitative verification of the elemental composition of the nanoalloys was done using EDX as shown in Fig. 6. The EDX spectra of AgAuNPs-GSH, and AuAgNPs-GSH (Fig. 6) showed the presence of Au, Ag, C, N, S and O peaks. The intensity of the gold and silver peaks in the spectra, clearly show the abundance of each element in the alloy. Residual potassium was observed in the EDX spectra of AgAuNPs-GSH and AuAgNPs-GSH due to the KOH that was used in the functionalization of the NPs with glutathione. The EDX spectrum of AgAu-SiNPs-APTES (Fig. 6) showed the presence of Au, Ag, Si, C, N, S and O, confirming their presence in alloy.

### 3.1.6. XPS analysis

The XPS survey spectra for AgAuNPs, AgAu-SiNPs-APTES exhibited the expected atomic compositions with their corresponding binding energies, Fig. 7, Table 2. XPS provides valuable chemical state information on the surface of the material being studied and was employed in this work to further confirm the coating of AgAuNPs with

SiNPs. Comparing the atomic concentrations of AgAuNPs and AgAu-SiNPs, a significant decrease in Ag and Au concentration was observed in the latter compared to former. This occurrence could be due to grafting of AgAuNPs into the pores of the SiNPs, hence preventing the efficient assessment of the AgAuNPs in the AgAu-SiNPs-APTES. The increase in the atomic concentration of O in Table 2 for AgAu-SiNPs compared to AgAuNPs also confirms the presence of O rich SiNPs on top of AgAuNPs, while the decrease in C is a result of less C in SiNPs covering AgAuNPs, the latter containing C rich OA/OLA.

### 3.2. Photophysical parameters

Table 1 compares the fluorescence quantum yields ( $\Phi_F$ ) and lifetimes ( $\tau_F$ ), triplet quantum yields ( $\Phi_T$ ) and lifetimes ( $\tau_T$ ), and singlet oxygen quantum yields ( $\Phi_\Delta$ ) of complex 1 alone, 1-AgAu-SiNPs-APTES, 1-AgAuNPs-GSH and 1-AuAgNPs-GSH in DMSO and in water (the latter for  $\Phi_F$  and  $\Phi_\Delta$  only).

#### 3.2.1. Fluorescence quantum yields ( $\Phi_F$ ) and lifetimes ( $\tau_F$ )

A fluorescence decay curve for 1-AgAuNPs-GSH in DMSO is shown in Fig. 8, as an example. The MPC alone afforded a mono-exponential decay profile indicating one fluorescence lifetime. All the nanoconjugates showed bi-exponential fluorescence lifetimes. The bi-exponential fluorescence lifetimes observed in the nanoconjugates could be due to

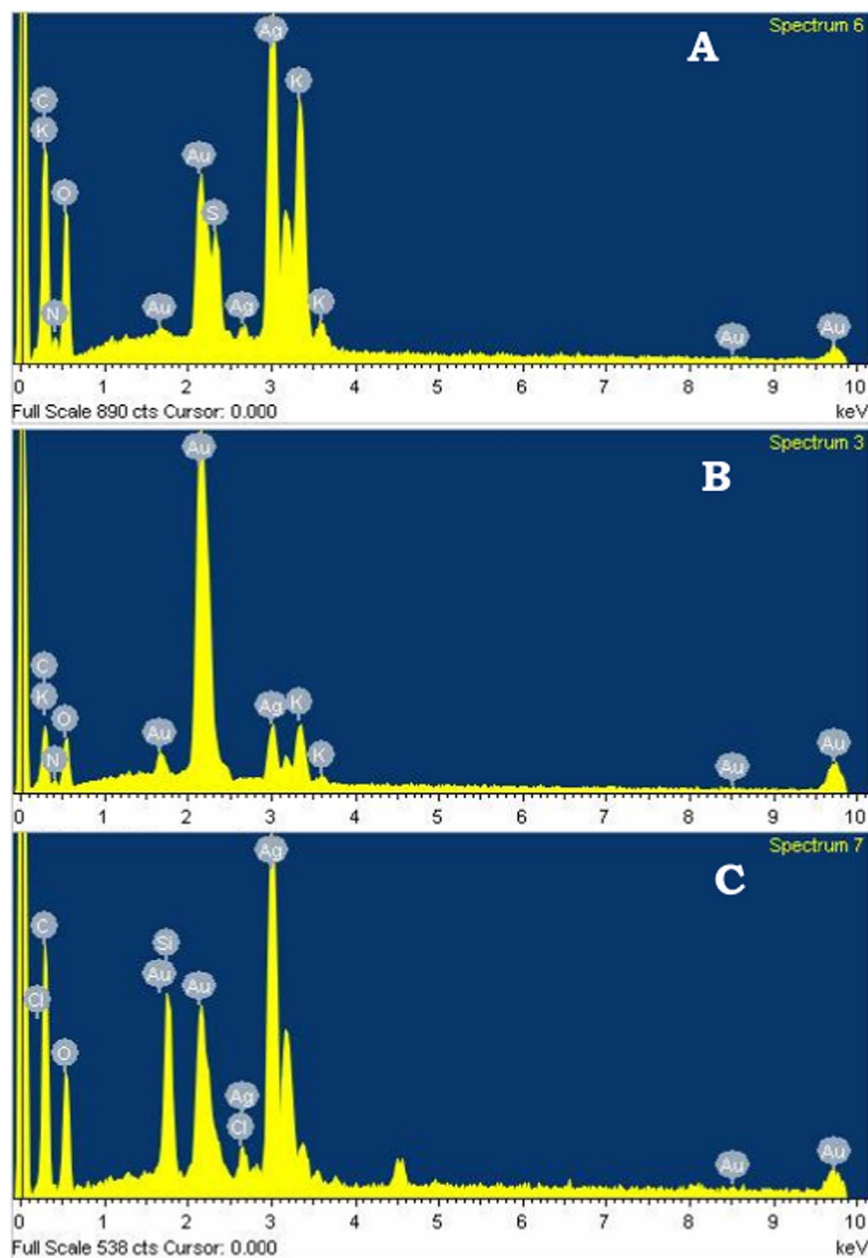


Fig. 6. EDX spectra of AgAuNPs-GSH (A), AuAgNPs-GSH (B), AgAu-SiNPs-APTES (C).

the orientation of the MPC around the NPs [39]. It has been reported that when a fluorophore (MPC) is in close proximity to a metal (NPs), the fluorophore interacts with the free electrons on the surface of the metal modifying its fluorescence behaviour [40].

As shown in Table 1, the fluorescence quantum yield and lifetime of complex 1 in DMSO decreased on conjugation to NPs and this could be attributed to the heavy atom effect of the latter, which promotes intersystem crossing to the triplet state [41], lowering fluorescence. The fluorescence quantum yields in DMSO are higher than in water (Table 1). The low values in water are attributed to aggregation which usually quenches fluorescence. Aggregates are known to convert electronic excitation energy to vibrational energy which consequently decreases the fluorescence quantum yield of molecules [40].

### 3.2.2. Triplet quantum yields ( $\Phi_T$ ) and lifetimes ( $\tau_T$ )

Fig. 9 shows the triplet decay curve for 1-AuAgNPs-GSH in DMSO (as an example). 1-AgAuNPs-GSH and 1-AuAgNPs-GSH showed increased  $\Phi_T$  values in comparison to complex 1 alone. As earlier stated,

heavy atom effect of the NPs enhance intersystem crossing to the triplet state, hence increasing the  $\Phi_T$  values of the nanoconjugates as compared to complex 1 alone [41]. 1-AuAgNPs-GSH containing more Au (a heavier atom than Ag), has a larger  $\Phi_T$  value compared to 1-AgAuNPs-GSH. The lengthening of lifetimes for complex 1 in the presence of the AuAgNPs may be due to the protection of the former by the latter. There was however, no change in lifetime in the presence of AgAuNPs. It is possible that the larger AuAgNPs (18.9 nm) protected complex 1 more effectively than the smaller AgAuNPs (15.1 nm). For 1-AgAu-SiNPs-APTES, a decrease in  $\Phi_T$  is observed when compared to complex 1 alone. We have reported [42] a decrease in  $\Phi_T$  values when PCs are covalently linked to SiNPs, possibly due to PCs interlinking with the SiNPs, resulting in the quenching of the excited states. The  $\Phi_T$  value for 1-AgAu-SiNPs-APTES, is however still reasonably high at 0.55 allowing for the conjugate to still be used for photosensitization. 1-AgAu-SiNPs-APTES has the longest lifetime in Table 1, suggesting more protection of the PCs by SiNPs. The triplet quantum yield of complex 1 and its nanoconjugates could not be obtained in water due to

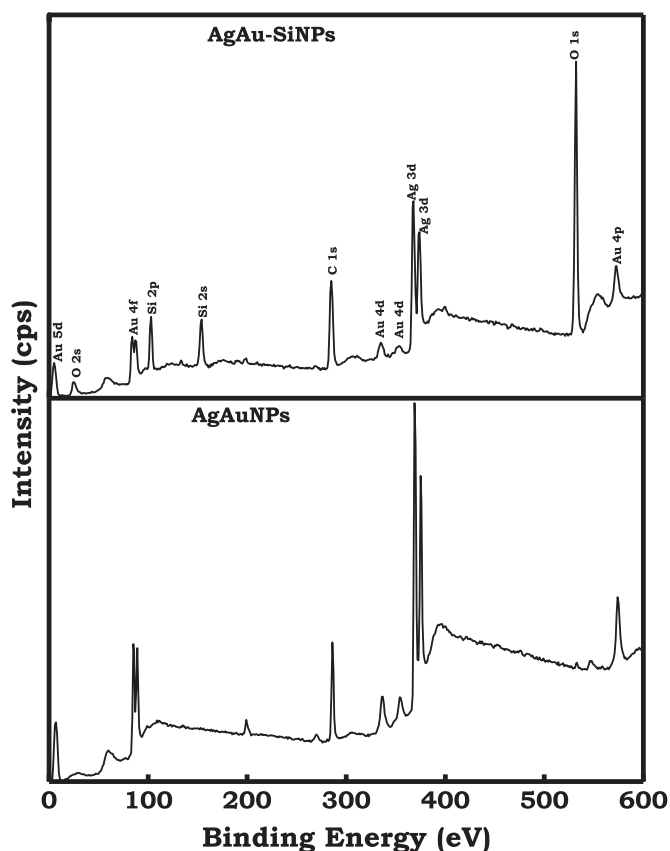


Fig. 7. XPS spectra survey spectra for AgAuNPs and AgAu-SiNPs.

**Table 2**  
XPS apparent surface composition of SiNPs, AgAuNPs and AgAu-SiNPs-APTES.

Samples	Atomic concentration (%)				
	C	O	Si	Ag	Au
AgAuNPs-OA/OLA	82.51	1.90	N/A	11.54	3.81
AgAu-SiNPs-APTES	36.38	40.77	24.33	2.78	0.77

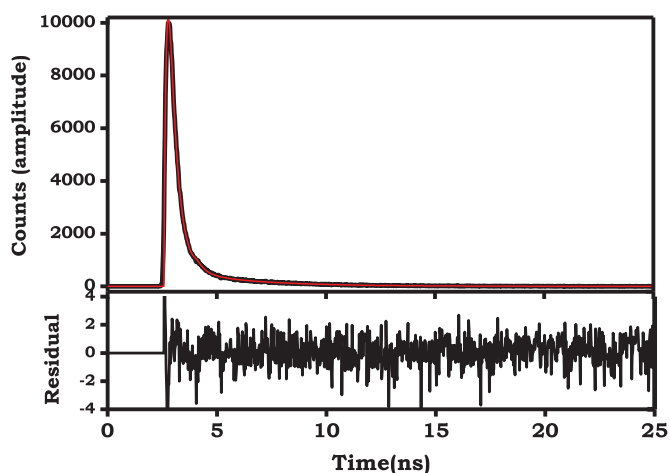


Fig. 8. Fluorescence decay curve for 1-AgAuNPs-GSH.

aggregation.

### 3.2.3. Singlet oxygen quantum yields

The singlet oxygen quantum yields were determined in DMSO using DPBF (and ADMA in water) as singlet oxygen quenchers. On

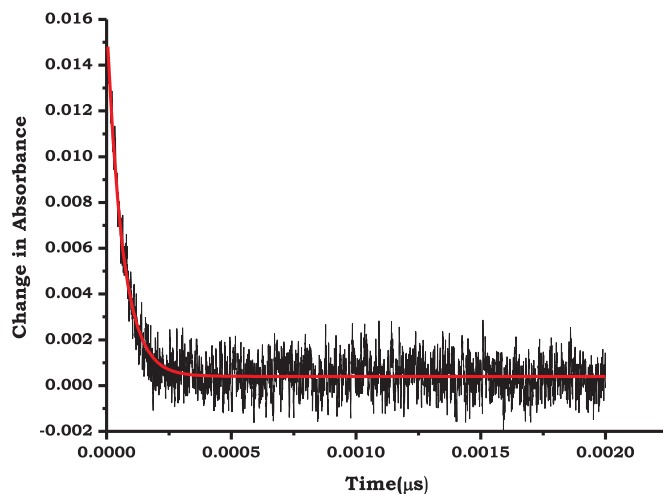
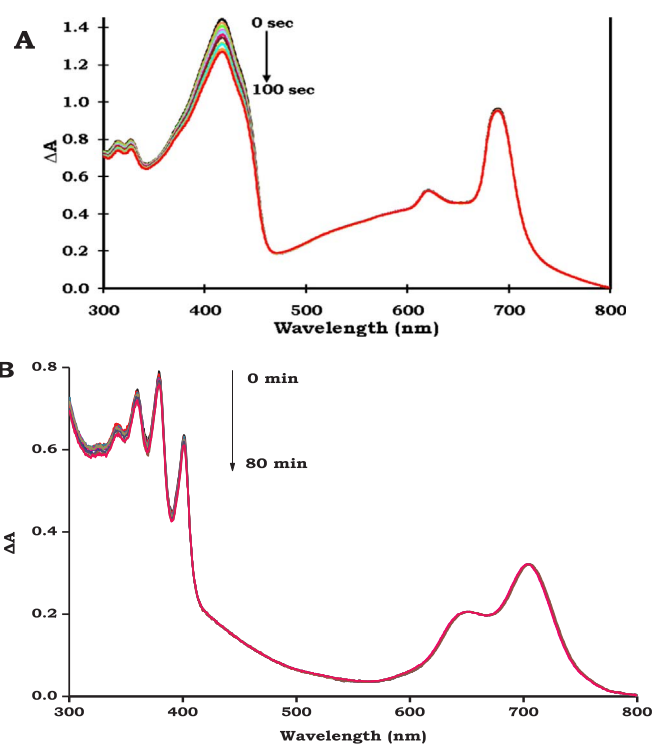


Fig. 9. Triplet absorption decay curve for 1-AuAgNPs-GSH in DMSO.



**Fig. 10.** Representative spectra for singlet oxygen quantum yield determination using a photochemical method. The spectra show the degradation of (A) DPBF ( $6.0 \times 10^{-5}$  M) in the presence of 1-AgAuNPs-GSH ( $9.8 \times 10^{-6}$  M) in DMSO and (B) ADMA ( $5 \times 10^{-5}$  M) in the presence of 1-AgAu-SiNPs-APTES ( $5.0 \times 10^{-6}$  M) in water (containing a few drops of DMSO).

irradiation, the Q-band of complex 1 and its nanoconjugates was unchanged except the depletion of the DPBF (or ADMA) over the time course, Fig. 10 (using 1-AgAuNPs-GSH in DMSO and 1-AgAu-SiNPs-APTES in water as examples).

A good photosensitizer should have high triplet and singlet oxygen quantum yields [43]. As shown in Table 1, 1-AgAu-SiNPs-APTES in DMSO, displayed increased singlet oxygen quantum yield compared to 1 and other conjugates. Conjugates 1-AgAuNPs-GSH and 1-AuAgNPs-GSH, showed lower singlet oxygen quantum yield than complex 1, and the values do not correspond to increased triplet quantum yields. Production of singlet oxygen is dependent on the triplet state population and the effectiveness of energy transfer process between the excited triplet state of the photosensitizer and ground state molecular oxygen [34,44]. The decrease in the singlet oxygen quantum

yield for 1–AgAuNPs–GSH and 1–AuAgNPs–GSH could be due to the screening effect caused by the capping ligand around the surface of the NPs which could have prevented the interaction of the excited triplet state of the nanoconjugates and the ground state molecular oxygen [45,46]. The higher singlet oxygen quantum yield for 1–AgAu–SiNP–s–APTES could probably be due to the permeability of the porous silica matrix to molecular oxygen [36,47]. Hence linking phthalocyanines to AgAuNPs contained within a SiNPs matrix is advantageous for production of singlet oxygen which is essential for application of the nanoconjugates for areas such as PDT.

The singlet oxygen quantum yield for complex 1 and its nanoconjugates in water were lower than in DMSO (Table 1). In addition to aggregation in water, the weak singlet oxygen quantum yield could be because water quenches singlet oxygen [28]. Even though the values are low, the conjugates can still be used for PDT since complexes such as lutetium texaphyrin with a low singlet oxygen value of 0.11 have been employed for clinical application in PDT [1]. The singlet oxygen quantum yield of 1–AgAuNPs in water could not be determined because the absorption peak of ADMA could not be seen since it overlapped with that of the silver SPR peak. The SPR peak of 1–AgAuNPs in water is very large (at 1 absorbance) compared to that of the Q band (~ 0.1 absorbance) (as shown in Fig. 2B).

#### 4. Conclusions

In this work, the conjugation of AuAgNPs–GSH, AgAuNPs–GSH and AgAu–SiNPs–APTES with indium(III) chloride 2,9(10),16(17),23(24)–tetra–(3–carboxyphenoxy)phthalocyanine (1) is reported. The nanoconjugates formed were characterized using XRD, TEM, XPS, FTIR and UV/vis spectra. In addition, the photophysical behavior of 1 and the nanoconjugates was studied. The singlet oxygen quantum yield for 1–AgAuNPs–GSH and 1–AuAgNPs–GSH was lower than that of the MPC alone however 1–AgAu–SiNPs–APTES had an increased singlet oxygen quantum yield in DMSO.

#### Acknowledgements

This work was supported by the Department of Science and Technology (DST) and National Research Foundation (NRF), South Africa through DST/NRF South African Research Chairs Initiative for Professor of Medicinal Chemistry and Nanotechnology (UID 62620) as well as Rhodes University.

#### References

- [1] R. Bonnett, In *Chemical Aspects of Photodynamic Therapy*, Gordon and Breach Science Publishers, Amsterdam, 2000.
- [2] S.B. Brown, E.A. Brown, I. Walker, The present and future role of photodynamic therapy in cancer treatment, *Lancet Oncol.* 5 (2004) 497–508.
- [3] I. Okura, *Photosensitization of Porphyrins and Phthalocyanines*, Gordon and Breach Publishers, Germany, 2001.
- [4] S. Liu, G. Chen, P.N. Prasad, M.T. Swihart, Synthesis of monodisperse Au, Ag, and Au–Ag alloy nanoparticles with tunable size and plasmon resonance frequency, *Chem. Mater.* 23 (2011) 4098–4101.
- [5] S. Besner, M. Meunier, Femtosecond laser synthesis of AuAg nanoalloys: photo-induced oxidation and ions release, *J. Phys. Chem. C* 114 (2010) 10403–10409.
- [6] A.S. Nair, V. Suryanarayanan, T. Pradeep, J. Thomas, M. Anija, R. Philip, Au<sub>x</sub>Ag<sub>y</sub>@ZrO<sub>2</sub> core-shell nanoparticles: synthesis, characterization, reactivity and optical limiting, *Mater. Sci. Eng. B* 117 (2005) 173–182.
- [7] S. Dengler, C. Kubel, A. Schwenke, G. Ritt, B. Eberle, Near- and off-resonant optical limiting properties of gold–silver alloy nanoparticles for intense nanosecond laser pulses, *J. Opt.* 14 (2012) 075203–075211.
- [8] I. Papagiannouli, P. Aloukos, D. Rioux, M. Meunier, S. Couris, Effect of the composition on the nonlinear optical response of Au<sub>x</sub>Ag<sub>1-x</sub> nano-alloys, *J. Phys. Chem. C* 119 (2015) 6861–6872.
- [9] G.A. Sotiriou, G.D. Etterlin, A. Spyrogiani, F. Krumeich, J.C. Leroux, S. Pratsinis, Plasmonic biocompatible silver–gold alloyed nanoparticles, *Chem. Commun.* 50 (2014) 13559–13562.
- [10] A.Q. Wang, J.H. Liu, S.D. Lin, T.S. Lin, C.Y. Mou, A novel efficient Au–Ag alloy catalyst system: preparation, activity, and characterization, *J. Catal.* 233 (2005) 186–197.
- [11] D.I. Kondarides, X.E. Verykios, Interaction of oxygen with supported Ag–Au alloy

- catalysts, *J. Catal.* 158 (1996) 363–377.
- [12] L. Tong, M. Claire, C.M. Cobley, J. Chen, Y. Xia, J.X. Cheng, Bright three-photon luminescence from gold/silver alloyed nanostructures for bioimaging with negligible photothermal toxicity, *Angew. Chem. Int. Ed.* 49 (2010) 3485–3488.
- [13] K.S. Abhijith, R. Sharma, R. Ranjan, M.S. Thakur, Facile synthesis of gold–silver alloy nanoparticles for application in metal enhanced bioluminescence, *Photochem. Photobiol. Sci.* 13 (2014) 986–991.
- [14] M.E. Wieder, D.C. Hone, M.J. Cook, M.M. Handsley, J. Gavrilovic, D.A. Russell, Intracellular photodynamic therapy with photosensitizer–nanoparticle conjugates: cancer therapy using a 'Trojan horse', *Photochem. Photobiol. Sci.* 5 (2006) 727–734.
- [15] M. Camerin, M. Magaraglia, M. Soncin, G. Jori, G.M. Moreno, I. Chambrier, M.J. Cook, D.A. Russell, The in vivo efficacy of phthalocyanine–nanoparticle conjugates for the photodynamic therapy of *amelanotic melanoma*, *Eur. J. Cancer* 46 (2010) 1910–1918.
- [16] N. Nombona, K. Maduray, E. Antunes, A. Karsten, T. Nyokong, Synthesis of phthalocyanine conjugates with gold nanoparticles and liposomes for photodynamic therapy, *J. Photochem. Photobiol. B: Biol.* 107 (2012) 35–44.
- [17] N. Nombona, E. Antunes, C. Litwinski, T. Nyokong, Synthesis and photophysical studies of phthalocyanine–gold nanoparticle conjugates, *Dalton Trans.* 40 (2011) 11876–11884.
- [18] T.P. Mthethwa, S. Tuncel, M. Durmuş, Tebello Nyokong, Photophysical and photochemical properties of a novel thiol terminated low symmetry zinc phthalocyanine complex and its gold nanoparticles conjugate, *Dalton Trans.* 42 (2013) 4922–4930.
- [19] N. Masilela, T. Nyokong, The interaction of silver nanoparticles with low symmetry cysteinyl metallophthalocyanines and their antimicrobial effect, *J. Photochem. Photobiol. A: Chem.* 255 (2013) 1–9.
- [20] O.M. Bankole, O. Osifeko, T. Nyokong, Enhanced nonlinear optical responses of zinc diaminopyrimidin-2-ylthio phthalocyanine conjugated to Ag<sub>x</sub>Au<sub>y</sub> alloy nanoparticles, *J. Photochem. Photobiol. A: Chem.* 329 (2016) 155–166.
- [21] T. Tran, T. Nguyen, *Functional Inorganic Nanohybrids for Biomedical Diagnosis*, InTech Publisher, Croatia, 2012.
- [22] M. Ambroz, A. Beeby, A.J. McRobert, M.S.C. Simpson, R.K. Svensen, D. Phillips, Preparative, analytical and fluorescence spectroscopic studies of sulphonated aluminium phthalocyanine photosensitizers, *J. Photochem. Photobiol. B: Biol.* 9 (1991) 87–95.
- [23] D.O. Oluwole, T. Nyokong, Comparative photophysical behavior of nanoconjugates of indium tetracarboxyphenoxy phthalocyanines covalently linked to CdTe/ZnSe/ZnO quantum dots, *J. Photochem. Photobiol. A: Chem.* 312 (2015) 34–44.
- [24] A. Fashina, E. Antunes, T. Nyokong, Characterization and photophysical behavior of phthalocyanines when grafted onto silica nanoparticles, *Polyhedron* 53 (2013) 278–285.
- [25] N. Zamand, A.N. Pour, M.R. Housaindokht, M. Izadyar, Size-controlled synthesis of SnO<sub>2</sub> nanoparticles using reverse microemulsion method, *Solid State Sci.* 33 (2014) 6–11.
- [26] G. Sanchez, D. Curiel, I. Ratera, A. Tarraga, J. Veciana, P. Molina, Modified mesoporous silica nanoparticles as a reusable, selective chromogenic sensor for mercury(II) recognition, *Dalton Trans.* 42 (2013) 6318–6326.
- [27] S. Fery-Forgues, D. Lavabre, Modified mesoporous silica nanoparticles as a reusable, selective chromogenic sensor for mercury (II) recognition, *J. Chem. Educ.* 76 (1999) 1260–1264.
- [28] A. Ogunsipe, J.Y. Chen, T. Nyokong, Photophysical and photochemical studies of zinc (II) phthalocyanine derivatives – effects of substituents and solvents, *New J. Chem.* 28 (2004) 822–827.
- [29] T.H. Tran-Thi, C. Desforge, C. Thiec, S.J. Gaspard, Singlet–singlet and triplet–triplet intramolecular transfer processes in a covalently linked porphyrin–phthalocyanine heterodimer, *J. Phys. Chem.* 93 (1989) 1226–1233.
- [30] N.A. Kuznetsova, N.S. Gretsova, O.A. Yuzhakova, V.M. Negrimovskii, O.L. Kaliya, E.A. Luk'yanets, New reagents for determination of the quantum efficiency of singlet oxygen generation in aqueous media, *Russ. J. Gen. Chem.* 71 (2001) 36–41.
- [31] W. Spiller, H. Kliesch, D. Wöhrle, S. Hackbarth, B. Roder, G. Schnurpfeil, Singlet oxygen quantum yields of different photo-sensitizers in polar solvents and micellar solutions, *J. Porphyr. Phthalocyanines* 2 (1998) 145–158.
- [32] T. Nyokong, E. Antunes, Photochemical and photophysical properties of metallophthalocyanines (chapt. 34), in: K.M. Kadish, K.M. Smith, R. Guilard (Eds.), *The Handbook of Porphyrin Science*, 7 World Scientific, Singapore, 2010, pp. 247–349.
- [33] M.J. Stillman, T. Nyokong, in: C.C. Leznoff, A.B.P. Lever (Eds.), *Phthalocyanines: Properties and Applications*, vol. 1, VCH Publishers, New York, NY, 1989, (Chapter 3).
- [34] K.G. Thomas, P.V. Kamat, Chromophore functionalized gold nanoparticles, *Acc. Chem. Res.* 36 (2003) 888–898.
- [35] W. Freyer, S. Müller, K.J. Teuchner, Photophysical properties of benzoannulated metal-free phthalocyanines, *J. Photochem. Photobiol. A* 163 (2004) 231–240.
- [36] M.H. Majles Ara, Z. Dehghani, R. Sahraei, A. Daneshfar, Z. Javadi, F. Divsar, Diffraction patterns and nonlinear optical properties of gold nanoparticles, *J. Quant. Spectrosc. Radiat. Transf.* 113 (2012) 366–372.
- [37] M.A. Majeed Khan, Sushil Kumar, Maqsood Ahamed, Salman A. Alrokayana, M.S. Alsalia, Mansour Alhoshana, Structural and spectroscopic studies of thin film of silver nanoparticles, *Appl. Surf. Sci.* 257 (2011) 10607–10612.
- [38] R. Jenkins, R.L. Snyder, *Introduction to X-ray Diffraction*, Wiley and Sons, New York, 1996, p. 1998.
- [39] C.D. Geddes, *Topics in Fluorescence Spectroscopy*, in: J.R. Lakowicz (Ed.), Springer, New York, 2005 as cited in: M. Ledwaba et al. *J. Mol. Catal. A: Chem.* 403, 2015, pp. 64–76.

- [40] J.A. Lacey, D. Philips, Fluorescence lifetime measurements of disulfonated aluminium phthalocyanine in the presence of microbial cells, *Photochem. Photobiol. Sci.* 1 (2002) 378–383.
- [41] Y. Shimzu, T. Azumi, Mechanism of external heavy atom effect on intersystem crossing in fluid solutions. Analysis based on fluorescence decay data, *J. Phys. Chem.* 86 (1982) 22–26.
- [42] A. Fashina, E. Antunes, T. Nyokong, Photophysical behavior of Zn aminophenoxy substituted phthalocyanine conjugates with carboxylic acid-coated silica nanoparticles: effect of point of substitution, *J. Mol. Struct.* 1068 (2014) 245–254.
- [43] Alexandra B. Ormond, Harold S. Freeman, Dye sensitizers for photodynamic therapy, *Materials* 6 (2013) 817–840.
- [44] E.I. Sagun, E.I. Zenkevich, V.N. Knyukshuto, A.M. Shulga, D.A. Starukhin, C. von Borczyskowski, Interaction of multiporphyrin systems with molecular oxygen in liquid solutions: extra-ligation and screening effects, *Chem. Phys.* 275 (2002) 211–230.
- [45] S.J. Chadwick, D. Salah, P.M. Livesey, M. Brust, M. Volk, Singlet oxygen generation by laser irradiation of gold nanoparticles, *J. Phys. Chem. A* 120 (2016) 10647–10657.
- [46] R. Yin, T. Agrawal, U. Khan, G.K. Gupta, V. Rai, Y.Y. Huang, M.R. Hamblin, Antimicrobial photodynamic inactivation in nanomedicine: small light strides against bad bugs, *Nanomedicine* 10 (2015) 2379–2404.
- [47] Y.Y. Huang, S.K. Sharma, T. Dai, H. Chung, A. Yaroslavsky, M. Garcia-Diaz, J. Chang, L. Chiang, M. Hamblin, Can nanotechnology potentiate photodynamic therapy? *Nanotechnol. Rev.* 10 (2012) 111–146.